

Evidence for strong electron–phonon coupling and polarons in the optical response of $\text{La}_{2-x}\text{Sr}_x\text{CuO}_4$

Oleg V Dolgov

P. N. Lebedev Physical Institute, 117924 Moscow, Russia.

Holger J Kaufmann and Ekhard K H Salje

Interdisciplinary Research Centre in Superconductivity, University of Cambridge, Madingley Road, Cambridge CB3 0HE, UK and Department of Earth Sciences, University of Cambridge, Downing Street, Cambridge CB2 3EQ, UK.

Yoad Yagil*

Interdisciplinary Research Centre in Superconductivity, University of Cambridge, Madingley Road, Cambridge CB3 0HE, UK

Abstract

The normal state optical response of $\text{La}_{2-x}\text{Sr}_x\text{CuO}_4$ is found to be consistent with a simple multi-component model, based on free carriers with strong electron–phonon interaction, localized polaronic states near 0.15 eV and a mid-infrared band at 0.5 eV. Normal state reflectance and absorbance of $\text{La}_{1.83}\text{Sr}_{0.17}\text{CuO}_4$ are investigated and their temperature dependence is explained. Both, the ac and dc response are recovered and the quasi-linear behavior of the optical scattering rate up to $3000 - 4000 \text{ cm}^{-1}$ is found to be consistent with strong electron–phonon interaction, which also accounts for the value of T_c . Although not strictly applicable in the superconducting state, our simple model accounts for the observed penetration depth and the optical response below T_c can be recovered by introducing a small amount of additional carriers. Our findings suggest that the optical response of $\text{La}_{2-x}\text{Sr}_x\text{CuO}_4$ could be explained both, in the normal and superconducting state, by a simple multi-fluid model with strong electron–phonon interaction if the gap symmetry and the temperature dependence of the 0.5 eV MIR band are adequately taken into account.

74.20.De, 74.25Fy, 74.25Gz, 74.72Dn

Typeset using REVTeX

I. INTRODUCTION

Experimental studies in recent years have revealed a variety of anomalous optical properties of high temperature superconductors (HTSC), both in the normal and superconducting state, which are still not fully understood theoretically. The optical conductivity in the mid- and near-infrared (MIR,NIR) regimes in the metallic phase of these materials is unusually high. The temperature dependence is extremely weak and the superconducting transition can hardly be observed at far-infrared (FIR) frequencies. In addition, powder absorbance measurements^{1–3} reveal an unusual temperature dependence of the integrated absorbance in the mid-infrared: An increase in the integrated absorbance upon cooling up to T_c is followed by a sharp slope change at T_c , and a saturation or even a decrease at lower temperatures. Such behavior can neither be explained by a normal Fermi–liquid approach nor by conventional strong-coupling theory.⁴

To explain the optical response of HTSC two main approaches are considered: single- and multi-component models. In single-component models the complex optical conductivity $\sigma(\omega)$ is written by means of a Drude term with both relaxation time τ and effective electron mass m^*/m being functions of the photon energy $\hbar\omega$,⁵

$$\sigma(\omega) = \frac{\omega_p^2}{4\pi} \frac{1}{1/\tau(\omega) - i\omega m^*(\omega)/m} , \quad (1)$$

while multi-fluid models⁶ generally include a number of Lorentz oscillators, peaked at non-zero frequencies. I.e. localized states which dominate at MIR frequencies are superimposed on a free carrier contribution in multi-component models. Experimental data on the optical conductivity of optimal doped HTSC compounds cannot distinguish between the above approaches since no clear structures are resolved in these data. In the case of underdoped compounds more structure is observed, suggesting that multi-component descriptions are more adequate.³

A vastly enhanced MIR response of chemically doped parent compounds of HTSC, both n type and p type, is also observed in the isolating state.^{7,8} Here the optical response

indicates the existence of self-localized carriers: small polarons. The MIR band, which is normally absent in stoichiometric samples, can be interpreted as a composition of overtones of local modes created by the self-trapping of extra charges injected into the lattice. In addition, absorbance measurements of various Sr doped $\text{La}_{2-x}\text{Sr}_x\text{CuO}_4$ (LSCO) compounds demonstrated that localized states are present near 0.15 eV and have a significant oscillator strength even at high doping levels.³ These results show that multi-component approaches should be considered in the under- and optimal doped regime, and even in slightly overdoped compounds.

So far multi-component approaches have used a simple Drude term to model the free carriers contribution to the optical response. However, there is considerable evidence for strong electron-phonon coupling in HTSC, and it is now widely accepted that the simple Fermi liquid quasiparticle description is not even applicable to the normal state metallic phase of these materials. Indeed, while the MIR spectra depend only weakly on temperature, the free carrier scattering rate, dominated by the electron-phonon interaction, is strongly temperature dependent and recent studies on $\text{YBa}_2\text{Cu}_3\text{O}_{7-\delta}$ (YBCO)⁹ and LSCO³ show that to model this behavior the simple Drude term for the free carriers must be modified to contain complicated frequency and temperature dependencies which yet have to be explained theoretically.

In this paper we will advance the multi-fluid approach by applying strong-coupling theory to determine the free carriers contribution to the optical response. As a model system we chose LSCO which is highly qualified for studying the optical properties of HTSC since it has no Cu-O chains and low c-axis conductivity. Analysis of absorbance data of under- and optimal doped compounds is straightforward using effective medium approach^{3,9}, since the c-axis conductivity is non metallic. For slightly overdoped LSCO, discussed here, c-axis conductivity might effect the FIR response but not the MIR and NIR spectra.

We will show that the normal state response of LSCO compounds is well described by a simple multi-component approach based on three main contributions: (a) free carriers response with strong electron-phonon interaction; (b) localized polaronic states near 0.15 eV;

(c) mid-infrared band near 0.5 eV. With this model one can account for the optical response and its temperature dependence, the dc resistivity, and the value of the superconducting transition temperature T_c based on normal electron-phonon interaction pairing.

Although a variety of simplifying assumptions make our model strictly applicable only in the normal state, it is instructive to apply it to the superconducting state as well. The predicted London penetration depth is in agreement with measured data and the optical response below T_c can be accounted for if a small amount of additional charge carriers, “hidden” in the normal state, is introduced. As the most likely source of these carriers we identified the 0.5 eV MIR band. This is in agreement with observed behavior of the total absorbance and would suggest a bipolaronic origin of this band, as proposed by Alexandrov *et al* (Ref. 10). Furthermore, an investigation of the FIR regime below T_c suggests that the gap-symmetry in LSCO is more complicated than simple s-wave, in agreement with earlier results (See for example H. S. Somal *et al* (Ref. 11) and references therein). Our findings indicate that the optical response of LSCO, and possibly of other HTSC, could be understood both, above and below T_c , within the framework of strong electron-phonon coupling theory if more realistic models for the 0.5 eV MIR band and the gap symmetry are used.

II. MODEL

We model the optical response within a three liquid model, consisting of two bands of localized charge carriers near 0.15 eV and 0.5 eV, respectively, and a free carrier contribution derived within the classical strong-coupling theory of superconductivity. If we disregard the phonon contribution in the FIR regime, the total dielectric function can be written as

$$\epsilon = \epsilon_\infty + \epsilon_E + \epsilon_{be_1} + \epsilon_{be_2} . \quad (2)$$

Here, ϵ_{be_1} and ϵ_{be_2} represent the contributions of the two MIR bands, 0.15 eV and 0.5 eV, respectively, and ϵ_E is the free carriers contribution.

In the normal state, with which we are mainly concerned here, the omission of phonons from the dielectric function has no substantial effect. We note however, that their omission magnifies the impact of the superconducting transition on the optical response below T_c . In order to include phonons one should consider their temperature dependent line width, energy shift, and renormalization below T_c which are out of the scope of the present paper.

The 0.15 eV band has been experimentally identified to be of polaronic origin^{3,12} since its optical activation energy is 3-5 times larger than the thermal one. The optical response of polarons depends on their size and on the distribution of binding energies, for example due to disorder, and might be well approximated by a Lorentzian dielectric function. We therefore model the 0.15 eV band with a temperature dependent Lorentz oscillator. It should be noted, however, that this approximation might be over-stretched in the FIR regime, especially for temperatures below T_c . According to the experimental results of Falck *et al* (Ref. 12) the polarons are thermally delocalized, hence we consider thermally activated charge transfer from the 0.15 eV band to free charge carriers.

The origin of the second MIR band, near 0.5 eV, is yet unknown. One possibility is the dissociation of bipolarons which do or do not form a conduction band. Experimentally it was shown that this band is only weakly temperature dependent and that the total absorbance is modified below the superconducting transition. In this work we ignore this temperature dependence since it is hardly observed in reflectance data, and approximate the 0.5 eV band with a temperature independent Lorentzian. Although this simplification is well justified in the normal state, there is evidence that it does not hold in the superconducting state.

The Lorentz dielectric functions for the two MIR bands have the form

$$\epsilon_{\text{be}_j}(\omega) = \frac{\omega_{\text{p}(\text{be}_j)}^2}{\omega_{\text{e}_j}^2 - \omega^2 - i\omega\gamma_{\text{e}_j}}, \quad j = 1, 2. \quad (3)$$

If we neglect any difference in effective mass between the polaronic and free states, the free carriers plasma frequency and the oscillator strength of the polaronic Lorentzian obey the sum rule

$$\omega_{\text{p}_\text{E}}^2(T) + \omega_{\text{p}(\text{be}_1)}^2(T) = \text{const.} \quad (4)$$

and the temperature dependent spectral weight of the 0.15 eV band is given by

$$\omega_{p_{(be_1)}}^2(T) = \omega_{p_{(be_1)}}^2(0) \left[1 - \exp\left(-\frac{T_0}{T}\right) \right], \quad (5a)$$

while the plasma frequency of the free carriers is

$$\omega_{p_E}^2(T) = \omega_{p_E}^2(0) + \omega_{p_{(be_1)}}^2(0) \exp\left(-\frac{T_0}{T}\right). \quad (5b)$$

Here, T_0 denotes a thermal activation energy.

The free carriers contribution to the optical response is calculated by applying conventional strong-coupling theory. Thus, we assume that the conduction electrons in the Cu–O planes behave like in a conventional electron–phonon superconductor, which can be treated by Migdal–Eliashberg theory, and for simplicity we assume s-wave pairing. The latter assumption is of course an oversimplification which might effect the FIR spectra below T_c . In this strong coupling extension of BCS theory expressions for the optical conductivity, disregarding vertex corrections for the electron–phonon interaction, are well established now.^{4,13–15} They require the solutions of the Eliashberg equations.¹⁶ For a two-dimensional isotropic system with cylindrical Fermi surface the Eliashberg equations for the renormalized gap parameter $\tilde{\Delta}$ and energy $\tilde{\epsilon}$ can be written in the following form¹⁴

$$\tilde{\epsilon}(\epsilon) = 1 - \int_{-\infty}^{\infty} d\omega \int_0^{\infty} d\Omega \alpha^2 F(\Omega) I(\epsilon + i\delta, \Omega, \omega) \operatorname{Re} \frac{\tilde{\epsilon}(\omega)}{\sqrt{\tilde{\epsilon}^2(\omega) - \tilde{\Delta}^2(\omega)}} , \quad (6a)$$

$$\begin{aligned} \tilde{\Delta}(\epsilon) = & - \int_{-\infty}^{\infty} d\omega \int_0^{\infty} d\Omega \alpha^2 F(\Omega) I(\epsilon + i\delta, \Omega, \omega) \operatorname{Re} \frac{\tilde{\Delta}(\omega)}{\sqrt{\tilde{\epsilon}^2(\omega) - \tilde{\Delta}^2(\omega)}} \\ & - \frac{1}{2} \mu^*(\omega_c) \int_{-\omega_c}^{\omega_c} d\omega \tanh \frac{\omega}{2T} \operatorname{Re} \frac{\tilde{\Delta}(\omega)}{\sqrt{\tilde{\epsilon}^2(\omega) - \tilde{\Delta}^2(\omega)}} , \end{aligned} \quad (6b)$$

where

$$I(\epsilon + i\delta, \Omega, \omega) = \frac{N(\Omega) + 1 - f(\omega)}{\epsilon + i\delta - \Omega - \omega} + \frac{N(\Omega) + f(\omega)}{\epsilon + i\delta + \Omega - \omega} , \quad (7)$$

μ^* is the Coulomb pseudo-potential and ω_c is the frequency cutoff. $N(\Omega)$ and $f(\omega)$ are Bose and Fermi distribution functions. As usual, the impurities are assumed to be non-magnetic

here. Consequently, impurity scattering does not appear in the isotropic equations (6a) and (6b).

Using the standard theory of electromagnetic response function, the optical conductivity can subsequently be calculated in the local (London) limit. Therefore, the free carriers contribution to the optical conductivity is given by¹³

$$\sigma_E(\omega, T) = \frac{\omega_{pe}^2}{2\pi\omega} \int_{-\infty}^{\infty} d\epsilon \left[\tanh \frac{\epsilon}{2k_B T} M(\epsilon, \omega) \left(g(\epsilon)g(\epsilon + \omega) + h(\epsilon)h(\epsilon + \omega) + \pi^2 \right) \right. \\ \left. - \tanh \frac{\epsilon + \omega}{2k_B T} M^*(\epsilon, \omega) \left(g^*(\epsilon)g^*(\epsilon + \omega) + h^*(\epsilon)h^*(\epsilon + \omega) + \pi^2 \right) \right. \\ \left. + \tanh \frac{\epsilon + \omega}{2k_B T} L(\epsilon, \omega) \left(g^*(\epsilon)g(\epsilon + \omega) + h^*(\epsilon)h(\epsilon + \omega) + \pi^2 \right) \right. \\ \left. - \tanh \frac{\epsilon}{2k_B T} L(\epsilon, \omega) \left(g^*(\epsilon)g(\epsilon + \omega) + h^*(\epsilon)h(\epsilon + \omega) + \pi^2 \right) \right] , \quad (8)$$

where

$$g(\epsilon) = \frac{-\pi \tilde{\epsilon}(\epsilon)}{\sqrt{\tilde{\Delta}^2(\epsilon) - \tilde{\epsilon}(\epsilon)}} , \quad (9a)$$

$$h(\epsilon) = \frac{-\pi \tilde{\Delta}(\epsilon)}{\sqrt{\tilde{\Delta}^2(\epsilon) - \tilde{\epsilon}(\epsilon)}} . \quad (9b)$$

The functions

$$M(\epsilon, \omega) = \left[\sqrt{\tilde{\Delta}^2(\epsilon + \omega) - \tilde{\epsilon}^2(\epsilon + \omega)} + \sqrt{\tilde{\Delta}^2(\epsilon) - \tilde{\epsilon}^2(\epsilon)} + \gamma_{imp} \right]^{-1} , \quad (10a)$$

and

$$L(\epsilon, \omega) = \left[\sqrt{\tilde{\Delta}^2(\epsilon + \omega) - \tilde{\epsilon}^2(\epsilon + \omega)} + \sqrt{\tilde{\Delta}^{*2}(\epsilon) - \tilde{\epsilon}^{*2}(\epsilon)} + \gamma_{imp} \right]^{-1} , \quad (10b)$$

include normal impurity scattering effects in Born approximation, γ_{imp} is an average scattering rate, and ω_{pe}^2 denotes the effective plasma frequency of the free carriers in the Cu–O planes. The free carriers contribution to the total dielectric function (2) is then given by $\epsilon_E(\omega) = 4\pi i\sigma_E(\omega, T)/\omega$.

The strong-coupling theory is no first principle theory but requires definite assumptions on the Eliashberg function, $\alpha^2 F(\omega)$, and needs coupling parameters as an input. Here we started from published phonon density of state¹⁷ but found it incompatible with the

optical and the dc data since the scattering rate at low frequencies is too large. Better agreement is achieved when $\alpha(\omega)$ is nonuniform and increases at high frequencies. This is also consistent with tunneling data^{18,19} where high energy phonons seem to have stronger electron–phonon interaction coefficient. For the sake of simplicity we chose a power law behavior: $\alpha^2(\omega) = (\omega/\omega_0)^\eta$ with $\eta > 0$. The phonon spectrum $F(\omega)$ is estimated by a set of quadratic Lorentzians and a low frequency cutoff function to account for the low frequency tail which otherwise dominates the electron–phonon interaction constant

$$\lambda = 2 \int_0^\infty \frac{d\omega}{\omega} \alpha^2(\omega) F(\omega) . \quad (11)$$

The resulting Eliashberg function is shown in Fig. 1 and the parameters used to define $\alpha^2(\omega)F(\omega)$ are listed in Table I. The overall coupling coefficient λ was adjusted to give the correct value of T_c . To determine the superconducting transition temperature for our choice of parameters we used McMillan’s equation.²⁰ The resulting T_c is in good agreement with the transition temperature derived directly from Migdal–Eliashberg theory by calculating the London penetration depth $\lambda_L(T)$. In the superconducting state, for T close to T_c , one expects $\lambda_L^{-2}(T) \propto T_c - T$. Since

$$\lambda_L^{-2}(T) = \lim_{\omega \rightarrow 0} 4\pi\omega \operatorname{Im} \sigma(\omega, T) , \quad (12)$$

the transition temperature can be easily determined once $\sigma_E(\omega)$ is calculated. Similarly, the impurity scattering rate γ_{imp} is found by the measured dc resistivity, and the strength of localized states is in general agreement with those found in absorbance measurements.³

We have performed various model calculations using different values for the electron–phonon coupling strength λ , ranging from 0.7 – 1.4. These calculations show that it is necessary to assume $\lambda \approx 1$ to achieve reasonable agreement with both, tunneling data and the optical and dc data. In general, we found that the different kinds of data investigated here put severe constraints on possible choices of the fitting parameters and we note that although the number of model parameters is rather large, no significant deviation from the parameters listed below (Table II) are possible.

III. RESULTS AND DISCUSSION

Using the model described in Sec. II we have calculated the optical reflectance and dc resistivity of slightly overdoped $\text{La}_{2-x}\text{Sr}_x\text{CuO}_4$, $x = 0.17$. The calculated curves were then fitted to the experimental data of Gao *et al* (Ref. 21) at $T = 200$ K with the addition of a high frequency Lorentzian at 1.5 eV. The resulting fit parameters are listed in Table II. Figure 2 shows the calculated normal state reflectance,

$$R(\omega) = \left|(\epsilon^{1/2}(\omega) - 1)/(\epsilon^{1/2}(\omega) + 1)\right|^2, \quad (13)$$

together with the measured ones at three different temperatures and an additional calculated curve at 40 K. At low frequencies ($< 1000 \text{ cm}^{-1}$) the optical response is dominated by the free carriers and is therefore temperature dependent. At higher frequencies the temperature dependence is largely suppressed since the spectral weights of the two localized states become appreciable and since the opposite trends of the 0.15 eV band and the free carrier part result in partial compensation. At higher frequencies ($> 3000 \text{ cm}^{-1}$) the calculated spectrum is dominated by the 0.5 eV band and is practically temperature independent. The thermal activation energy of the 0.15 eV band, $T_0 = 500 \text{ cm}^{-1}$, is by roughly a factor of 4 smaller than the optical energy, indicating self-localized charge carriers: while the lattice is frozen for the fast optical transitions (Frank–Condon principle), in thermal excitations it has time to relax and the polaronic binding energy is consequently reduced. The activation energy $T_0 = 500 \text{ cm}^{-1}$ is very close to the polaronic energies found in insulating parent compounds of HTSC.^{7,8} Moreover, photoexcited carrier relaxation measurements by Mihailovic *et al* provide evidence for localized polaronic states at similar energies in both, LSCO and YBCO.²²

Another quantity of interest is the dielectric loss function, $\text{Im}(-1/\epsilon(\omega))$. Experimentally the loss function of HTSC is found to follow a quadratic behavior, $\text{Im}(-1/\epsilon(\omega)) \propto \omega^2$, over almost the entire frequency range up to the plasma edge, where it exhibits a (first) peak and subsequently decreases.²³ The height of the peak is temperature dependent, while its position and the curvature of $\text{Im}(-1/\epsilon(\omega))$ strongly depend on ϵ_∞ . We have calculated the

dielectric loss function using a variety of different model parameters, confirming the high sensitivity of the peak position to the choice of ϵ_∞ . For optimally doped ($x = 0.15$) LSCO the position of the maximum has been reported to be approximately 6500 cm^{-1} .²³ Figure 3 shows the dielectric loss function for $\text{La}_{1.83}\text{Sr}_{0.17}\text{CuO}_4$ at 200 K as calculated within our multi-liquid model using the parameters from Table II. The behavior in the FIR and MIR regimes is quadratic to good approximation and the curve shows a maximum at 6320 cm^{-1} , close to the experimentally observed value for optimal doping. This confirms our choice of $\epsilon_\infty = 4.43$.

With the parameters obtained from the fit of the reflectance data the absorption coefficient $\alpha(\omega) = 4\pi\omega\text{Im}(\epsilon^{1/2}(\omega))$ can be calculated and compared to measured optical absorbance data. Analysis of absorbance data must take into account grain-size effects and the response of the host material. Therefore, the major disadvantage of this approach is the difficulty in converting qualitative results into quantitative ones. However, it has been shown recently that absorbance measurements at MIR frequencies can be analyzed quantitatively within the framework of the effective medium approach.⁹ Figure 4 shows normal state powder absorbance data of $\text{La}_{1.83}\text{Sr}_{0.17}\text{CuO}_4$ from Ref. 3. In Fig. 5 the corresponding calculated curves are shown. In agreement with the experimental results, $\alpha(0\text{K}) - \alpha(300\text{K}) \approx 10^4\text{ cm}^{-1}$ near 0.15 eV. The overall behavior of the absorbance is well resembled in Fig. 5: All curves show the characteristic maximum close to the 0.5 eV band and the absorption coefficient decreases with increasing temperature for frequencies up to 3000 cm^{-1} .

The normal state response can also be described within the framework of an extended Drude model where the relaxation time τ and the effective mass m^* are allowed to vary with frequency. Writing the normal state optical conductivity derived within our three-liquid model in a generalized Drude formula, Eq. (1), the scattering rate $1/\tau$ and the effective mass m^*/m can be calculated. They are shown in Fig. 6, together with the "optical scattering rate",

$$\frac{1}{\tau^*} = \omega \frac{\text{Re}(\sigma)}{\text{Im}(\sigma)} = \frac{m}{m^*} \frac{1}{\tau} . \quad (14)$$

The quasi-linear behavior of $1/\tau^*$ up to $3000 - 4000 \text{ cm}^{-1}$ was one of the driving forces for assuming electron-electron interaction (marginal²⁴ and nested²⁵ Fermi Liquids for example) rather than electron-phonon one since the phonon spectrum does not exceed 1000 cm^{-1} . As already mentioned by Shulga *et al* (Ref. 26) this argument is valid for $1/\tau$ rather than $1/\tau^*$ which indeed becomes frequency independent above the phonon spectrum. Therefore the multi-component model with strong electron-phonon interaction supports one of the major properties of HTSC: the quasi-linear response of the optical scattering rate up to energies much higher than the phonon spectrum. It is important to note here that obtaining $1/\tau^*$ experimentally is somewhat delicate since this quantity is quite sensitive to the value of ϵ_∞ .

The general behavior of the dc resistivity also support the above picture, namely the co-existence of free and localized charge carriers and the thermal excitations of the later. Temperature dependent resistivity measurements are done at constant pressure, and the correction to constant volume reveal deviation from quasi-linear behavior where the resistivity data tend to saturate or follow a lower slope at high energies. This change of slope is also noticed in the calculated resistivity, where the larger number of free carriers reduces the slope of the $\rho(T)$ curve, Fig. 7. Another manifestation of the above behavior is the doping dependence of $d\rho/dT$. Uchida has measured the temperature dependence of several LSCO compounds up to 950 K.²⁷ A clear deviation from linear temperature dependence is observed at high temperatures for the $x = 0.1$ and $x = 0.12$ compounds even in the constant pressure data. Moreover, a rough estimate of the ratios between the slopes $[d\rho/dT]_x/[d\rho/dT]_{0.1}$ yields 0.1, 0.2, 0.36, 0.58 for $x = 0.3, 0.2, 0.15, 0.12$, respectively. Assuming that λ does not change much for these compounds one expects $d\rho/dT \propto 1/\omega_p^2 \propto 1/(x - x_0)$, where x_0 is the total number of localized carriers per Cu atom. The above ratios yield $x_0 = 0.075$ in close agreement with the estimated spectral weight from absorbance measurements.³

Once the parameters of our model are determined as described above, the optical response of LSCO can be calculated for arbitrary temperatures, above and below $T_c = 37.4 \text{ K}$. Therefore, we will also apply the model to the superconducting state to gain an insight in how it could and should be altered to be applicable in both, the normal and superconducting

state.

The first quantity of interest here is the London penetration depth. According to Eq. (12), its zero-temperature value, $\lambda_L(0)$, provides a measure for the free carriers plasma frequency $\omega_{pe}(0)$, since the zero-frequency limit of the conductivity is entirely due to the free carriers response. Figure 8 shows the normalized inverse penetration depth, $\lambda_L^2(0)/\lambda_L^2(T)$, as predicted by our three-liquid model, using the parameters from Table II. At low temperatures the phenomenological relation,

$$\lambda_L(T) \approx \lambda_L(0) \left[1 - \left(\frac{T}{T_c} \right)^4 \right]^{-1/2}, \quad (15)$$

is well resembled and we can use this expression to extrapolate $\lambda_L(T)$ to zero temperature. This yields $\lambda_L(0) = 2579 \text{ \AA}$. Experimentally it is difficult to obtain the absolute value of the penetration depth, especially for thin films. However, it is generally accepted that $\lambda_L(0) > 2300 \text{ \AA}$ for optimally doped LSCO²⁸⁻³⁰. Using muon spin relaxation rate measurements Aeppli *et al* found $\lambda_L(0) \approx 2500 \text{ \AA}$, close to the value predicted by our multi-liquid approach.

It has been observed earlier for various HTSC that the integrated absorbance exhibits an unusual temperature dependence.¹⁻³ In the normal state the integrated absorbance increases upon cooling. At the superconducting transition temperature a sudden slope change occurs, followed by a saturation or even a decrease of the integrated absorbance upon further cooling. Figure 9 shows the measured³ absorbance of 0.17 Sr LSCO integrated over the frequency range $1600 \text{ cm}^{-1} < \omega < 4500 \text{ cm}^{-1}$, normalized to unity at 40K. At low temperatures the experimental uncertainties are fairly large, but a saturation effect below T_c can clearly be seen. This indicates that spectral weight is shifted from the 0.5 eV band into the δ -peak at zero-frequency upon cooling below T_c . Within ordinary strong-coupling theory such behavior cannot be understood since $\omega \sim 0.5 \text{ eV} \gg 2\Delta$, and it should not be possible to reproduce this behavior within our multi-fluid model where the 0.5 eV MIR band has been assumed to be temperature-independent. Indeed, a saturation of the calculated total absorption coefficient can only be observed if the range of integration is extended well into the FIR regime, as shown in Fig. 10. This indicates that the observation of the superconducting

transition at NIR frequencies is not merely a result of Kramers–Kronig relations. The fact that an explanation of the observed change in integrated MIR absorbance is beyond our model suggests instead some temperature dependence of the 0.5 eV band and supports the approach of Alexandrov *et al* (Ref. 10).

Another discrepancy between the measured and calculated optical response can be seen in the reflectance below T_c . While the normal state fit curves practically coincide with the experimental reflectance data over a wide range of frequencies (see Fig. 2), in the superconducting state the measured reflectance from Gao *et al* is slightly underestimated by our model. This could be simply due to the fact that the simplifying assumption of equal effective mass for the free and localized carriers breaks down below T_c . Alternatively, the discrepancy can be accounted for by introducing additional free carriers. Figure 11 shows the measured reflectance at 10 K together with the prediction of our model. Here, a slightly modified model, with an additional small Drude term, with $\omega_{pD} = 2000 \text{ cm}^{-1}$ and $\gamma_D = 200 \text{ cm}^{-1}$, has been included. The close resemblance between the measured curve in Fig. 11 with this modified multi–liquid model indicates the existence of a “hidden” reservoir of charge carriers which has to be taken into account in the superconducting state. There is increasing evidence that the gap symmetry in LSCO is more complicated than simple s-wave.¹¹ In the case of d–wave pairing, the “hidden” carriers could be explained by the contribution of resonant scattering. Another likely source for these additional carriers is the second MIR band, near 0.5 eV, which was taken to be temperature independent in our simple multi–fluid approach. Indeed, by increasing the free carriers plasma frequency slightly, to $\omega_{pE}(0) = 10591 \text{ cm}^{-1}$, and decreasing the oscillator strength of the second Lorentzian accordingly, to $\omega_{p(b\epsilon 2)} = 5748 \text{ cm}^{-1}$, the MIR and NIR reflectance in the superconducting state can be easily accounted for. The consequent shift in spectral weight and the position of the second MIR band would then suggest a bipolaronic origin of this band. Alexandrov *et al* (Ref. 10) have shown that the unusual behavior of the integrated absorbance can be explained by Bose–condensation of bipolarons which are also responsible for the second MIR band. The comparison of our model with the measured reflectance in the superconducting

state seems to confirm this picture. In Fig. 12 the reflectance curve at 10 K calculated with the modified free carriers plasma frequency and oscillator strength of the second Lorentzian is shown for frequencies below 2500 cm^{-1} together with our original model and the measured reflectance. Above 1500 cm^{-1} the modified spectral weight provides better agreement with the experimental data. Between $100 - 600 \text{ cm}^{-1}$ our model predictions can be seen to deviate from the experimental curve, predicting lower absorbance in this frequency regime. This is due to the simplifying assumption of s-wave pairing for the free carriers. As mentioned above, the gap symmetry in LSCO is probably more complicated and must be taken into account to describe the FIR regime, since its shape leaves long tails which can easily alter the optical response up to 1000 cm^{-1} . In addition, the omission of phonon modes and the simplified model for the polaronic dielectric function also affects the FIR spectra, especially below T_c .

The correspondence of the normal state optical response of LSCO with the simple model consisting of a band of localized charge carriers, a temperature independent MIR band near 0.5 eV, and a free carrier contribution treated within ordinary strong coupling theory suggests the following physical picture for LSCO and possibly for other HTSC: The charge carriers introduced by doping in HTSC parent compounds are redistributed and form polaronic bound states. With increased doping levels, these states fill up to the overcrowding limit where additional bound states start to overlap existing ones. Additional doping results in the appearance of charge carriers which form a Fermi-liquid with strong electron-phonon interaction. The comparison of this model with experimental data in the superconducting state suggests further that (a) the gap symmetry in LSCO is more complicated than simple s-wave and (b) the broad MIR band at 0.5 eV might be of bipolaronic origin.

IV. SUMMARY

Our model, based on a free carrier response with strong electron-phonon interaction, localized polaronic states near 0.15 eV and a temperature independent mid-infrared band

near 0.5 eV reveals the following results: The normal state optical response of LSCO from the far-infrared to the near-infrared is consistent with our multi-liquid approach. Assuming strong electron-phonon coupling both the ac and dc response are recovered, the later up to very high temperatures. The quasi-linear behavior of the optical scattering rate for frequencies up to $3000 - 4000 \text{ cm}^{-1}$ is also consistent with this approach and in agreement with previous measurements³ we find the doping dependence $d\rho/dT \propto 1/(x - x_0)$, where $x_0 = 0.075$. The polaronic origin of the 0.15 eV band is confirmed. The temperature dependence of the optical response, both reflectance and absorbance, is explained and our model naturally accounts for the value of the superconducting transition temperature.

In the superconducting state the absolute value of the London penetration depth is recovered. A comparison of the calculated reflectance and integrated absorbance with measured data indicates that the simplifying assumption of a temperature independent mid-infrared band at 0.5 eV breaks down in the superconducting state. Model calculations would then suggest a bipolaronic origin of this band, in agreement with earlier results.¹⁰ Our model used the simplifying assumption of s-wave pairing. The far-infrared spectra suggest that the symmetry of the gap parameter is more complicated for LSCO. All this indicates that a multi-component approach can be extended to the superconducting state by more realistic models for both, the 0.5 eV mid-infrared band and the gap symmetry. Hence, the optical response of LSCO, both above and below T_c , could be understood within the framework of strong electron-phonon coupling theory which is also the driving mechanism for pairing if the localized states which dominate the mid-infrared response are adequately taken into account.

ACKNOWLEDGMENT

We gratefully acknowledge David Tanner for providing us with his reflectance data. One of us (H. J. K.) would like to thank V. V. Kabanov for many helpful discussions and O. V. D. would like to thank the Royal Society and the Department of Earth Sciences, University of

Cambridge for support and hospitality during the early stages of this work.

REFERENCES

* Permanent address: Intel Israel Ltd., M.T.M. Scientific Industries Centre, P.O.B. 1659 Haifa 31015, Israel.

¹ H. L. Dewing and E. K. H. Salje, *Supercond. Sci. Technol.* **5**, 50 (1992)

² C. H. Ruscher, M. Gotte, B. Schmidt, C. Quitmann, and G. Guntherodt, *Physica C* **204**, 30 (1992)

³ Y. Yagil and E. K. H. Salje, *Physica C* **256**, 205 (1996)

⁴ S. B. Nam, *Phys. Rev.* **156**, 470 and 487 (1967)

⁵ P. E. Sulewski, A. J. Sievers, M. B. Maple, M. S. Torikachvili, J. L. Smith, and Z. Fisk, *Phys. Rev. B* **38**, 5338, (1988)

⁶ T. Timusk, S. L. Herr, K. Kamaras, C. D. Porter, and D. B. Tanner, *Phys. Rev. B* **38**, 6683 (1988)

⁷ P. Calvani, M. Capizzi, S. Lupi, P. Maselli, and A. Paolone, in *Proceedings of the International Workshop on Anharmonic Properties of High-T_c Cuprates*, edited by D. Mihailović, G. Ruani, E. Kaldis, and K. A. Müller, (World Scientific, Singapore, 1994)

⁸ P. Calvani, M. Capizzi, S. Lupi, and G. Balestrino, *Europhys. Lett.* **31**, 473 (1995)

⁹ Y. Yagil, F. Baudenbacher, M. Zhang, J. R. Birch, H. Kinder, and E. K. H. Salje, *Phys. Rev. B* **52**, 1 (1995)

¹⁰ A. S. Alexandrov, A. M. Bratkovsky, N. F. Mott, and E. K. H. Salje, *Physica C* **215**, 359 (1993)

¹¹ H. S. Somal, B. J. Feenstra, J. Schützmann, Jae Hoon Kim, Z. H. Barber, V. H. M. Duijn, N. T. Hien, A. A. Menovsky, M. Palumbo, and D. van der Marel, *Phys. Rev. Lett.* **76**, 1525, (1996)

¹² J. P. Falck, A. Levy, M. A. Kastner, and R. J. Birgeneau, Phys. Rev. B **48**, 4043 (1993)

¹³ W. Lee, D. Rainer, and W. Zimmermann, Physica C **159**, 535 (1989)

¹⁴ O. V. Dolgov, A. A. Golubov, and S. V. Shulga, Phys. Lett. A **147**, 317 (1990)

¹⁵ R. Akis, J. P. Carbotte, and T. Timusk, Phys. Rev. B **43**, 12804 (1991)

¹⁶ G. M. Eliashberg, Zh. Eksp. Teor. Fiz. **38**, 966 (1960); Sov. Phys. — JETP **11**, 696 (1960)

¹⁷ B. Renker, F. Gompf, E. Gering, N. Nucker, D. Ewert, W. Reichardt, and H. Rietschel, Z. Phys. B **67**, 15 (1987)

¹⁸ L. N. Bulaevskii, O. V. Dolgov, I. P. Kazakov, S. N. Maksimovskii, M. O. Ptitsyn, V. A. Stepanov, and S. I. Vedeneev, Supercond. Sci. Technol. **1**, 205 (1988)

¹⁹ G. Deutscher, N. Hass, Y. Yagil, A. Revcolevschi, and G. Dhaleen, Journal of Superconductivity **7**, 371 (1994)

²⁰ P. B. Allen and B. Mitrović, Solid State Phys. **37**, 1, (1982)

²¹ F. Gao, D. B. Romero, and D. B. Tanner, Phys. Rev. B **47**, 1036 (1993)

²² D. Mihailović, T. Mertelj, B. Podobnik, J. Demsar, P. Canfield, Z. Fisk, and C. Chen, Physica B, **220**, 142 (1996)

²³ J. H. Kim, I. Bozovic, C. B. Eom, T. H. Geballe, and J. S. Harris, Physica C **174**, 435 (1991)

²⁴ C. M. Varma, P. B. Littlewood, S. Schmitt-Rink, E. Abrahams, and A. E. Ruckenstein, Phys. Rev. Lett. **63**, 1996 (1989); P. B. Littlewood and C. M. Varma, J. Appl. Phys. **69**, 4979 (1991)

²⁵ A. Virosztek and J. Ruvalds, Phys. Rev. B **42**, 4064 (1990); J. Ruvalds and A. Virosztek, J. Appl. Phys. **43**, 5498 (1991)

²⁶ S. V. Shulga, O. V. Dolgov, E. G. Maksimov, Physica C **178**, 226(1991); E. G. Maksimov,

S. Y. Savrasov, D. Y. Savrasov, and O. V. Dolgov, Phys. Rev. Lett. (submitted)

²⁷ S. Uchida, J. Phys. Chem. Solids **53**, 1603 (1992)

²⁸ W. J. Kossler, J. R. Kempton, X. H. Yu, H. E. Schone, Y. J. Uemura, A. R. Moodenbaugh, M. Suenaga, and C. E. Stronach, Phys. Rev. B **35** 7133 (1987)

²⁹ G. Aeppli, R. J. Cava, E. J. Ansaldo, J. H. Brewer, S. R. Kreitzman, G. M. Luke, D. R. Noakes, and R. F. Kiefl, Phys. Rev. B **35**, 7129 (1987)

³⁰ Y. J. Uemura, V. J. Emery, A. R. Moodenbaugh, M. Suenaga, D. C. Johnston, A. J. Jacobsen, J. T. Lewandowski, J. H. Brewer, R. F. Kiefl, S. R. Kreitzman, G. M. Luke, T. Riseman, C. E. Stronach, W. J. Kossler, J. R. Kempton, X. H. Yu, D. Opie, and H. E. Schone, Phys. Rev. B **38**, 909 (1988)

TABLES

TABLE I. Parameters used to define the Eliashberg function $\alpha^2 F(\omega)$. $\omega_{min} = 60$ cm $^{-1}$, $\omega_\alpha = 1000$ cm $^{-1}$, $A_\alpha = 3.8$, and $\eta = 1.9$, where: $\alpha^2(\omega) = A_\alpha(\omega/\omega_\alpha)^\eta$, $F(\omega) = \frac{2}{\pi} \tanh^{-1}((\omega/\omega_{min})^4) \sum_i A_i \left(1 + (\omega - \omega_{0i})^2/\omega_{d_i}^2\right)^{-2}$

| A | ω_0 | ω_d |
|------|------------|------------|
| 0.2 | 80 | 40 |
| 0.25 | 160 | 50 |
| 0.3 | 230 | 30 |
| 0.2 | 320 | 35 |
| 0.18 | 380 | 30 |
| 0.12 | 460 | 40 |
| 0.05 | 560 | 40 |
| 0.02 | 680 | 50 |

TABLE II. Parameters used to fit the optical and dc resistivity data of Gao *et al.* For $T > 250$ K the measured reflectance at high frequencies indicates a phase transformation. In order to account for this change in the calculation of the 300 K data we set $\epsilon_\infty = 3.9$ and $\omega_{p(b_{e_3})} = 9000$ cm $^{-1}$. No further changes were needed in order to fit the low and high temperature data.

| | |
|--------------------------|------------------|
| λ | 1.0 |
| μ^* | 0.05 |
| γ_{imp} | 100 cm $^{-1}$ |
| ϵ_∞ | 4.43 |
| T_0 | 500 cm $^{-1}$ |
| $\omega_{pE}(0)$ | 10400 cm $^{-1}$ |
| $\omega_{p(b_{e_1})}(0)$ | 7840 cm $^{-1}$ |
| ω_{e_1} | 1650 cm $^{-1}$ |
| γ_{e_1} | 3550 cm $^{-1}$ |
| $\omega_{p(b_{e_2})}$ | 5834 cm $^{-1}$ |
| ω_{e_2} | 3740 cm $^{-1}$ |
| γ_{e_2} | 5056 cm $^{-1}$ |
| $\omega_{p(b_{e_3})}$ | 6000 cm $^{-1}$ |
| ω_{e_3} | 11000 cm $^{-1}$ |
| γ_{e_3} | 5000 cm $^{-1}$ |

FIGURES

FIG. 1. Eliashberg function $\alpha^2 F(\omega)$ used to model the free carriers response of $\text{La}_{1.83}\text{Sr}_{0.17}\text{CuO}_4$. The corresponding parameters are listed in Table I.

FIG. 2. Measured²¹ and calculated reflectance of $\text{La}_{1.83}\text{Sr}_{0.17}\text{CuO}_4$ thick film. The fine structures at low frequencies (detailed scale, lower panel) are due to infrared phonons while the overall structure is due to strong electron–phonon interaction.

FIG. 3. Dielectric loss function $\text{Im}(-1/\epsilon)$ as a function of frequency for $\text{La}_{1.83}\text{Sr}_{0.17}\text{CuO}_4$ at 200 K as predicted by our three–liquid model.

FIG. 4. Measured³ powder absorbance (in absorbance units) for $\text{La}_{1.83}\text{Sr}_{0.17}\text{CuO}_4$ at various temperatures. The structure at 3700 cm^{-1} is an experimental artifact. On lowering the temperature the optical absorbance is enhanced over a wide frequency range.

FIG. 5. Absorption coefficient $\alpha(\omega) = 4\pi\omega \text{Im}\{\epsilon^{1/2}(\omega)\}$ for $\text{La}_{1.83}\text{Sr}_{0.17}\text{CuO}_4$ calculated within the multi–liquid model with strong electron–phonon interaction using the parameters from Table II.

FIG. 6. (top) Scattering rate $1/\tau$ and (middle) effective mass m^*/m in a generalized Drude model derived from our multi–fluid model. (bottom) The "optical scattering rate" $1/\tau^*$ derived within the multi–fluid model with strong electron–phonon interaction. While $1/\tau$ becomes practically frequency independent above the phonon spectrum $1/\tau^*$ shows quasi–linear behavior for frequencies up to $3000 – 4000 \text{ cm}^{-1}$.

FIG. 7. Calculated dc resistivity (solid line). The broken line indicates the dc resistivity without the delocalization of the 0.15 eV states, namely with constant number of free carriers.

FIG. 8. Normalized inverse London penetration depth as a function of reduced temperature, calculated from the optical conductivity as predicted by the multi–fluid model using the parameters from Table II. Also shown are the phenomenological curve $1 – (T/T_c)^4$ and a straight–line fit near $T_c = 37.4 \text{ K}$.

FIG. 9. Measured³ integrated absorbance for $\text{La}_{1.83}\text{Sr}_{0.17}\text{CuO}_4$, normalized to unity at 40K. The integration is over the spectral segment $1600 – 4500 \text{ cm}^{-1}$.

FIG. 10. Calculated absorption coefficient derived within the multi–liquid model using the parameters from Table II, integrated from $100 – 4500 \text{ cm}^{-1}$.

FIG. 11. Measured reflectance for $\text{La}_{1.83}\text{Sr}_{0.17}\text{CuO}_4$ at 10 K compared to our multi-fluid model, using the parameters from Table II (dash-dotted line). In contrast to the good agreement between data and fit in the normal state (compare Fig. 2), the measured reflectance at 10 K is slightly underestimated by our model. Also shown is a modified multi-fluid model (solid line), including an additional Drude term with $\omega_{\text{PD}} = 2000 \text{ cm}^{-1}$ and $\gamma_{\text{D}} = 200 \text{ cm}^{-1}$, which better resembles the measured reflectance.

FIG. 12. Comparison between the measured reflectance at 10 K, the multi-liquid model using the parameters from Table II (dotted line), and the model with weaker MIR response, $\omega_{\text{p}(\text{be}2)} = 5748.1 \text{ cm}^{-1}$ and $\omega_{\text{pE}}(0) = 10591 \text{ cm}^{-1}$ (solid line). The discrepancy in the FIR regime is due to various simplifying model assumptions, as explained in the text. Above 1500 cm^{-1} the measured data is well resembled by the modified model.

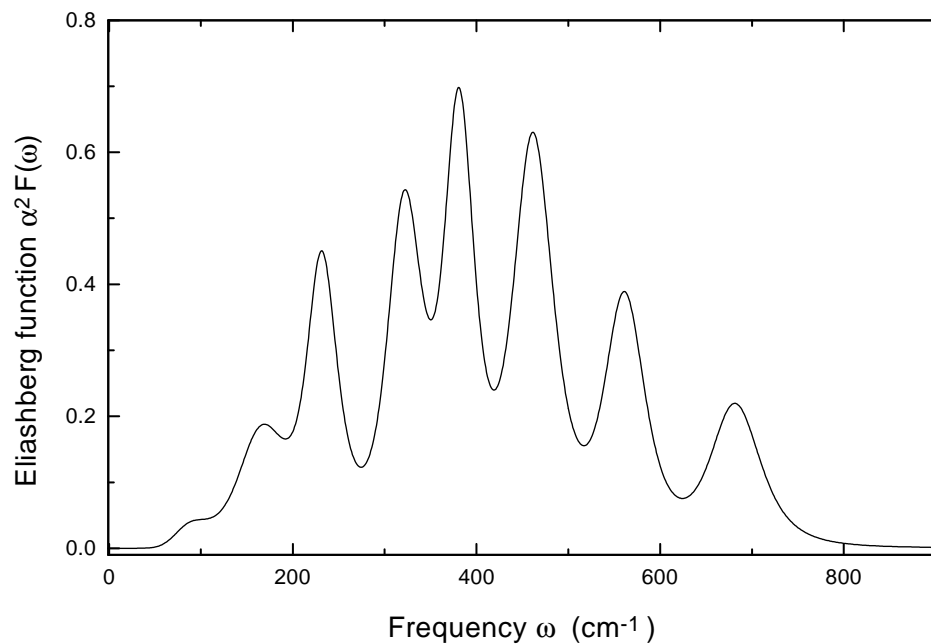


FIG. 1. Dolgov *et al*

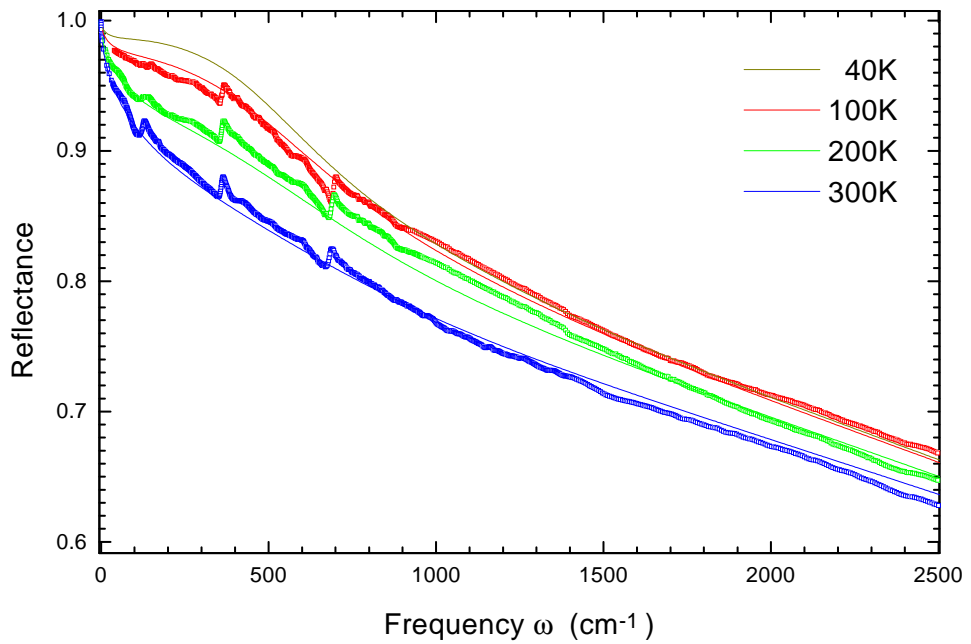
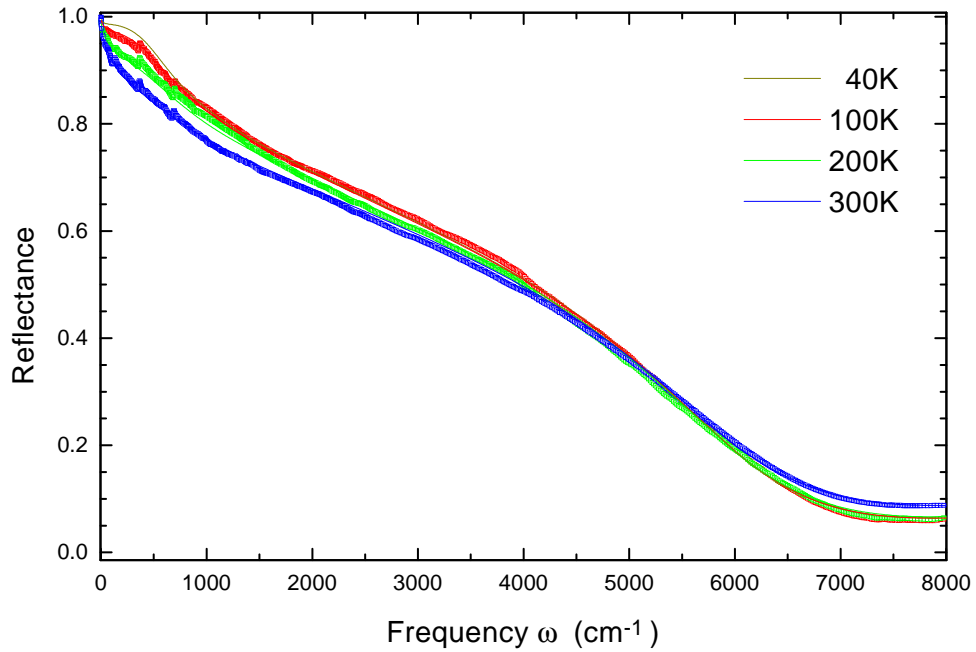


FIG. 2. Dolgov *et al*

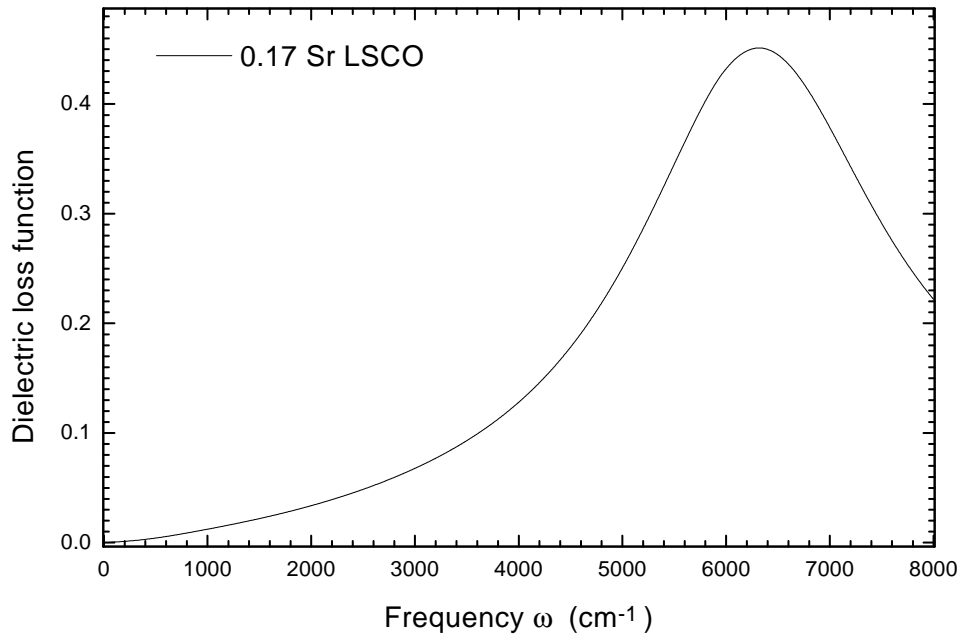


FIG. 3. Dolgov *et al*

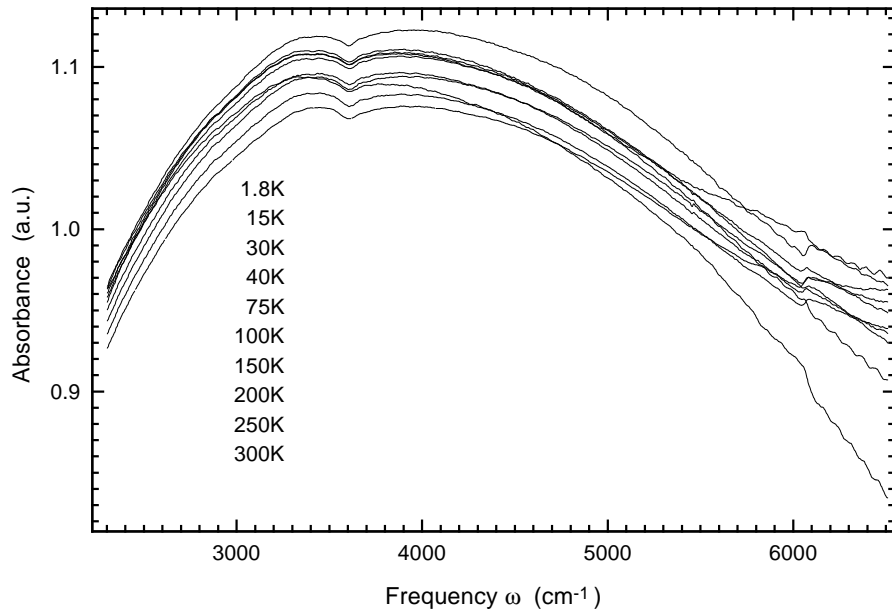


FIG. 4. Dolgov *et al*

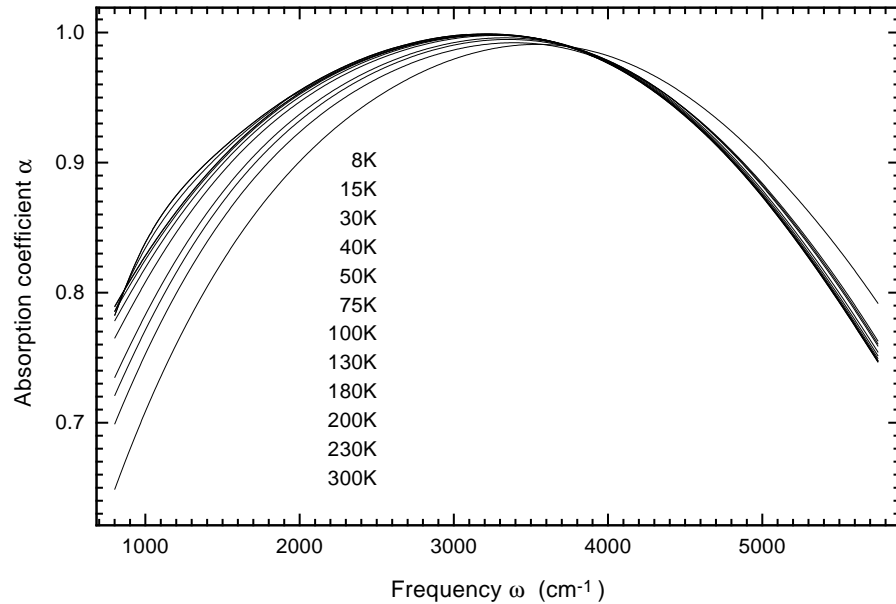


FIG. 5. Dolgov *et al*

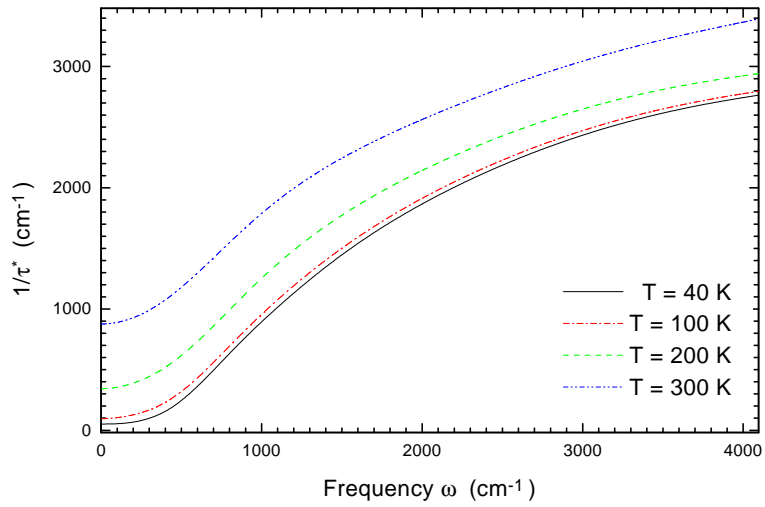
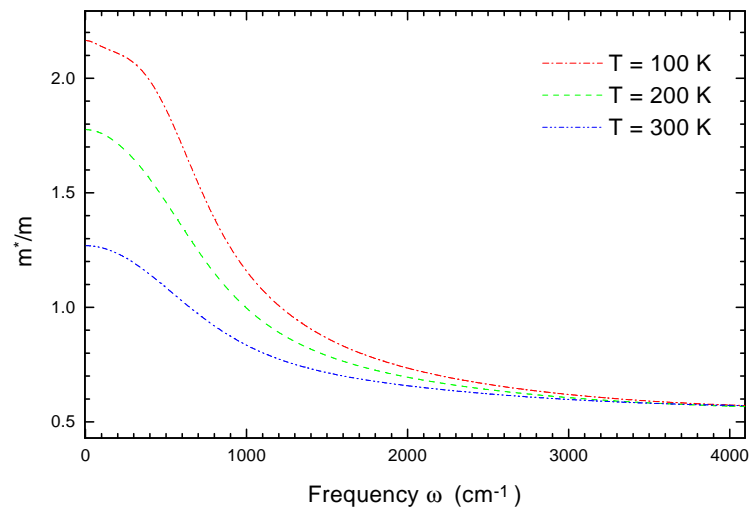
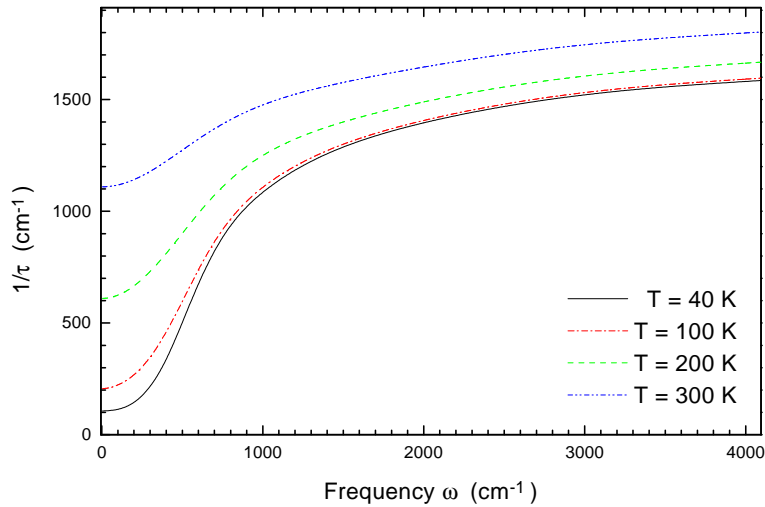


FIG. 6. Dolgov *et al*

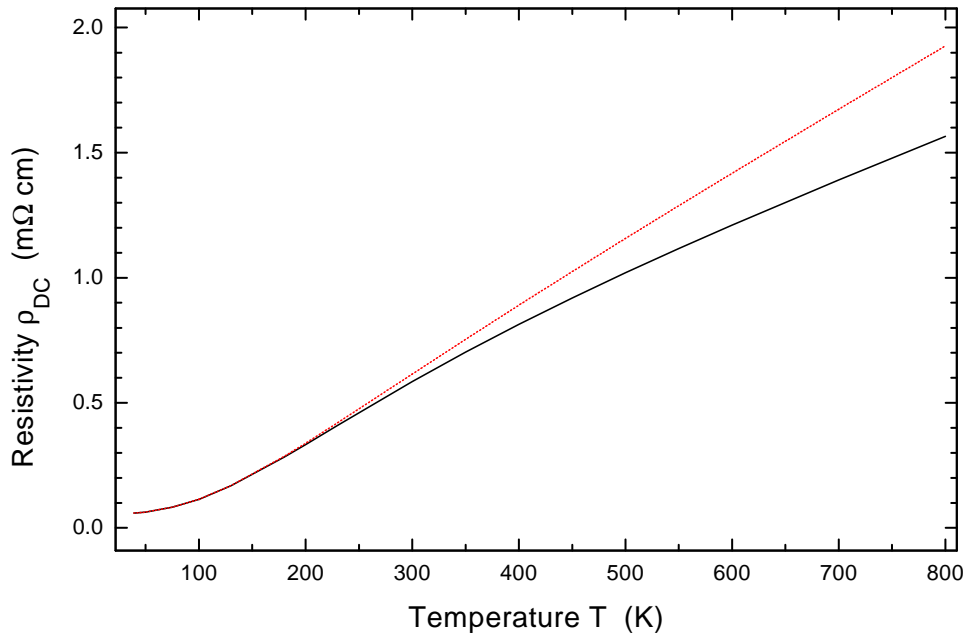


FIG. 7. Dolgov *et al*

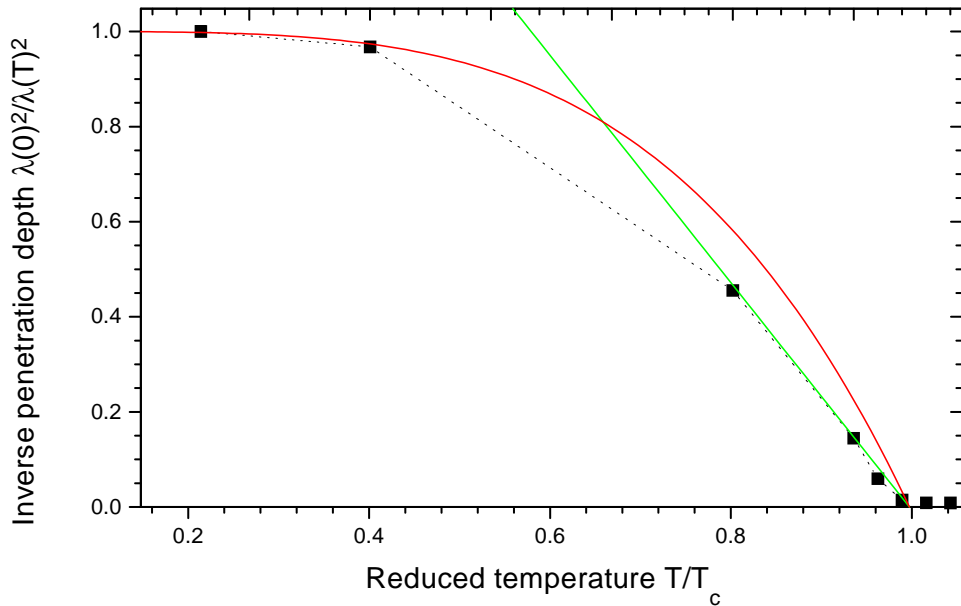


FIG. 8. Dolgov *et al*

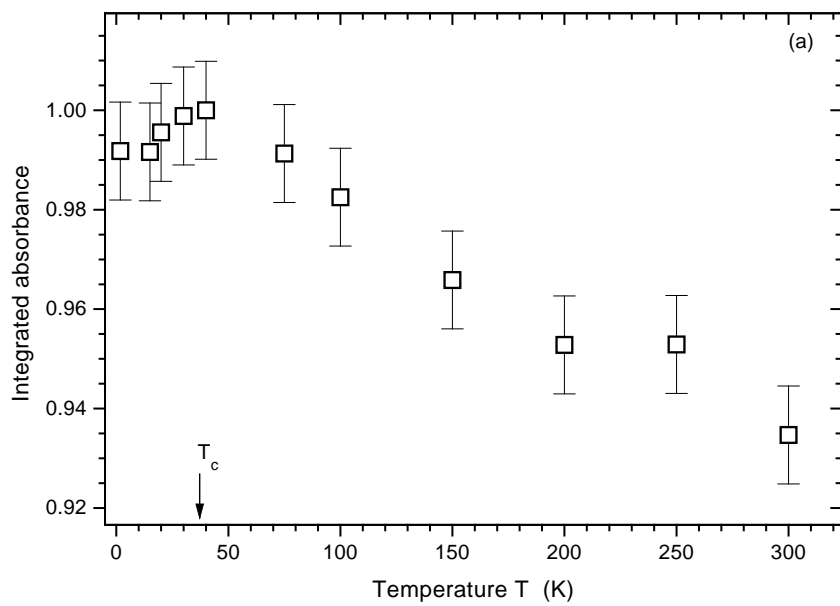


FIG. 9. Dolgov *et al*

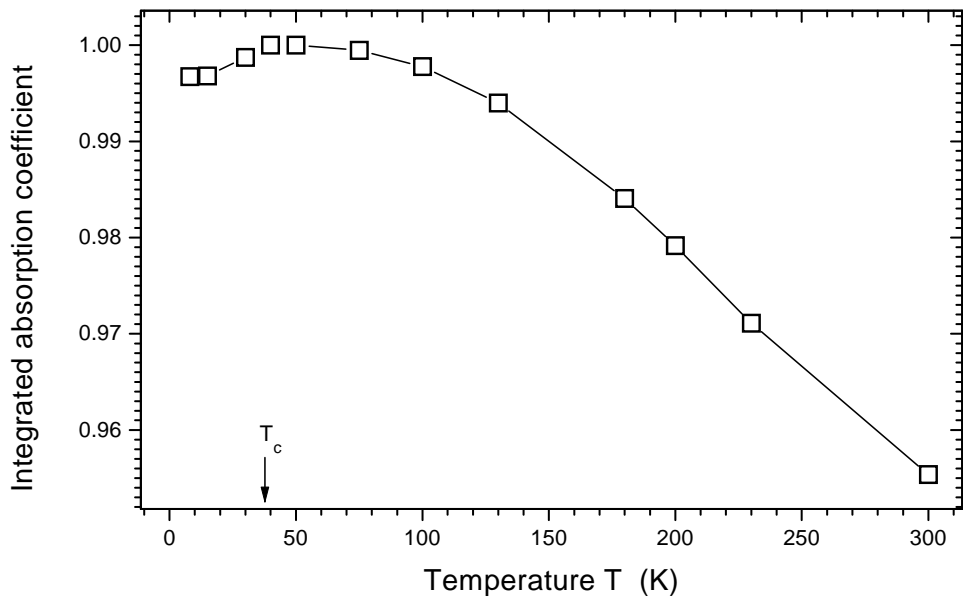


FIG. 10. Dolgov *et al*

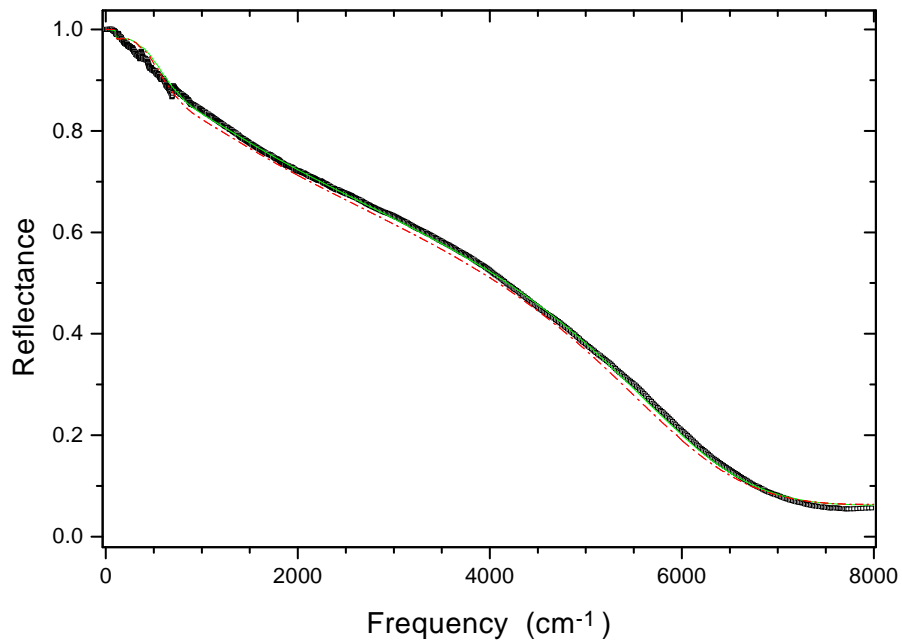


FIG. 11. Dolgov *et al*

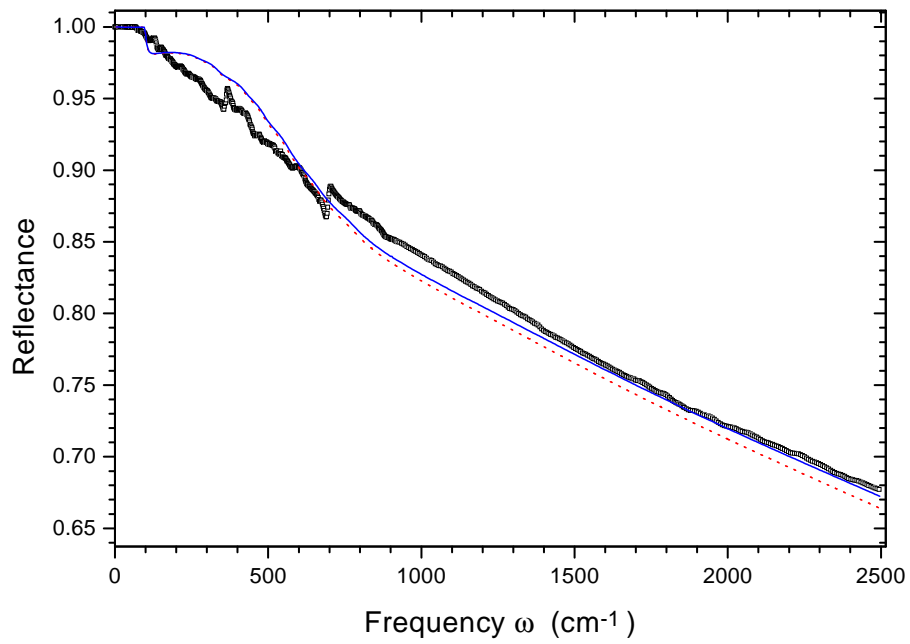


FIG. 12. Dolgov *et al*